

# Trade-off relation between strain dynamic range and spatial resolution in slope-assisted Brillouin optical correlation-domain reflectometry

Heeyoung Lee<sup>✉</sup>, Kohei Noda<sup>✉</sup>, Yosuke Mizuno<sup>✉</sup> and Kentaro Nakamura<sup>✉</sup>

Institute of Innovative Research, Tokyo Institute of Technology, Yokohama 226-8503, Japan

E-mail: [hylee@sonic.pi.titech.ac.jp](mailto:hylee@sonic.pi.titech.ac.jp)

Received 20 February 2019, revised 1 May 2019

Accepted for publication 20 May 2019

Published 4 June 2019



CrossMark

## Abstract

Slope-assisted Brillouin optical correlation-domain reflectometry (SA-BOCDR) is one of the high-speed distributed strain sensing techniques, but its strain dynamic range has been limited to approximately 0.15%, which is far from being sufficient for some practical applications. In this paper, we clarify that, unlike widely used time-domain techniques, SA-BOCDR has a trade-off relation between the strain dynamic range and the spatial resolution. This trade-off originates from the unique bell-shaped noise floor inherently involved in the Brillouin gain spectrum observed with correlation-domain techniques. We experimentally show that, at the cost of three times lowered spatial resolution, the strain dynamic range of >0.6% can be achieved.

Keywords: Brillouin scattering, distributed optical fiber sensor, strain dynamic range

(Some figures may appear in colour only in the online journal)

## 1. Introduction

Brillouin-scattering-based sensing [1] has been one of the most extensively studied topics in fiber-optic sensing community. It enables us to diagnose damaged civil infrastructures exploiting its capability of distributed strain/temperature measurement along fiber under tests (FUTs). Distributed Brillouin sensors are generally classified into two types: ‘analysis’ and ‘reflectometry’. In the former, two lightwaves need to be injected into both ends of an FUT, while in the latter, light injection to one end of an FUT is sufficient for proper operation. For each type, different schemes for acquiring position information, namely, time-[2–9], frequency-[10–13], and correlation-[5, 14–24] domain schemes, have been developed. Although different configurations have different merits and demerits, the target of this paper is Brillouin optical correlation-domain reflectometry (BOCDR), which is the only scheme with advantages such as single-end accessibility, random accessibility to sensing positions, and relatively high spatial resolution. To date, a number of configurations

of BOCDR have been implemented to achieve better sensing performance including spatial resolution [16–18], and measurement range [21, 22]. BOCDR suffered from its relatively long measurement time, but recently this issue has been mitigated by two frequency-sweeping-free configurations, called phase-detected (PD-) BOCDR [25] and slope-assisted (SA-) BOCDR [26]. Although PD-BOCDR has a high sampling rate of hundreds of kilohertz, its strain dynamic range is limited to approximately 0.2%. Though some attempts to extend the strain dynamic range have been made [27], it is still one of the major drawbacks of PD-BOCDR. Here, we concentrate attention on SA-BOCDR.

SA-BOCDR enables high-speed operation by exploiting the slope of the Brillouin gain spectrum (BGS). After demonstrating its basic operation [26], we have clarified its unique features such as beyond-nominal-resolution detectability [28] and adjustable sensitivity [29]. We have also shown its practical usefulness by providing a case example of distributed strain monitoring along an FUT embedded in a composite structure [30]. Remarkable progress has thus been made since

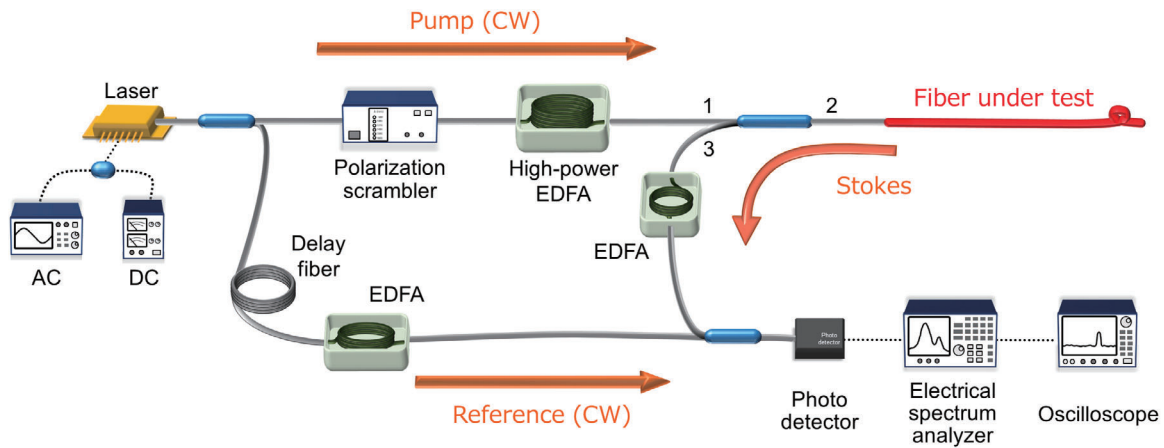


**Figure 1.** Experimental setup of SA-BOCDR. AC, alternating current; CW, continuous wave; DC, direct current; EDFA, erbium-doped fiber amplifier.

its first proposal, but one of the important problems unsolved yet is its strain (or temperature) dynamic range limited by the narrow linear range of the BGS slope. The linear range is generally reported to be several tens of megahertz [1], which corresponds to a relatively small strain of  $\sim 0.15\%$  (or temperature change of  $\sim 64$  K). This value is even lower than that of PD-BOCDR and is far from being sufficient for some practical applications [31–33].

The simplest idea to improve the strain dynamic range is to exploit not only the linear range but also the nonlinear range of the BGS. However, this approach may not operate so effectively as expected, because the BGS observed in BOCDR involves a unique bell-shaped background noise floor [34, 35], which is not sensitive to the strain applied to the sensing position. Thus, it is crucial to extend the upper limit of the measurable strain by another method.

In this work, to start with, we experimentally confirm that the aforementioned idea, i.e. additional use of the nonlinear range of the BGS, is not effective. The maximal measurable strain obtained by this approach is found to be merely  $\sim 0.25\%$ . Then, we clarify that SA-BOCDR has a trade-off relation between the strain dynamic range and the spatial resolution and that the former can be extended at the sacrifice of the latter. In the experiment, we achieve a strain dynamic range of  $>0.6\%$  when the spatial resolution is three times lower.

## 2. Principle

BOCDR operates based on correlation control of continuous lightwaves, which enables high spatial resolution and signal-to-noise ratio (SNR). By modulating the driving current of a light source, the optical frequency of its output is sinusoidally modulated to generate a ‘correlation peak’ in the FUT, which enables position-selective detection of Brillouin signal. By sweeping the modulation frequency  $f_m$ , the correlation peak can be scanned along the FUT for distributed measurement. Since multiple correlation peaks are generated periodically along the FUT, in a standard BOCDR configuration, the measurement range  $d_m$  is given by their interval as [36]

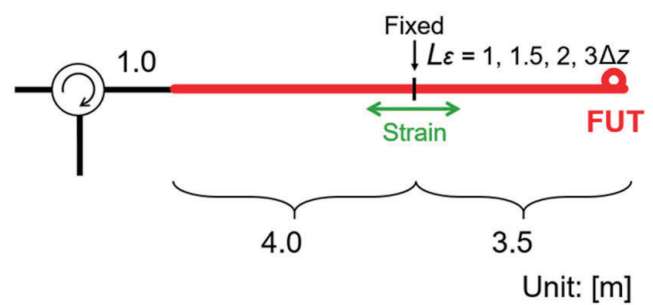


**Figure 2.** Structure of FUT.

$$d_m = \frac{c}{2nf_m}, \quad (1)$$

where  $c$  is the velocity of light in vacuum and  $n$  is the refractive index of the fiber core. The spatial resolution  $\Delta z$  is reported to be given by [36]

$$\Delta z = \frac{c\Delta\nu_B}{2\pi n f_m \Delta f}, \quad (2)$$

where  $\Delta\nu_B$  is the Brillouin bandwidth and  $\Delta f$  is the modulation amplitude of the optical frequency.

Brillouin-based sensing generally exploits the strain (or temperature) dependence of the Brillouin frequency shift (BFS) [1]. In standard BOCDR, the BFS is derived after acquiring the whole BGS, which is relatively time-consuming because optical frequency needs to be swept. In contrast, SA-BOCDR enables frequency-sweeping-free higher-speed operation by using, instead of the BFS itself, a spectral power  $P_{B0}$  at a certain frequency  $\nu_{B0}$  on the BGS slope. If we desire to measure tensile strain (or heat) applied to the FUT,  $\nu_{B0}$  is set to lower frequency than the BFS.

When SA-BOCDR was first developed, we determined the strain dynamic range by the linear range of the BGS slope [26]. It may be feasible to extend the dynamic range if the nonlinear range (foot of the BGS) is additionally used to measure strain at the cost of the deteriorated sensitivity. However, the effect of this method is probably limited because the BGS observed in BOCDR inherently involves a bell-shaped background noise

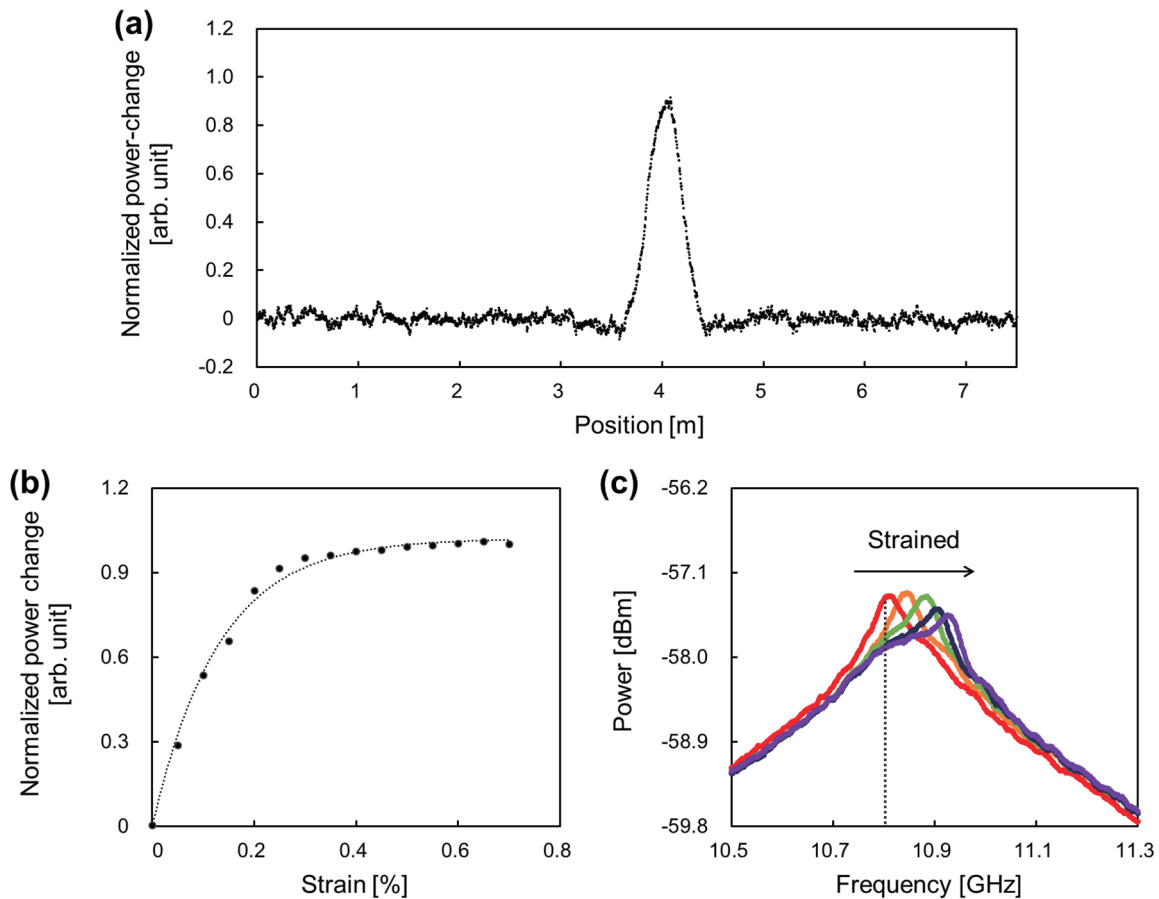


**Figure 3.** (a) Measured distribution of the normalized power change when the applied strain was 0.25%. (b) Normalized power change plotted as a function of applied strain. The dotted curve is an exponential fit. (c) BGSs measured at strains of 0, 0.1, 0.2, 0.25, 0.3% when the strained length  $L_e$  was the same as the nominal spatial resolution  $\Delta z$  ( $\approx -0.37$  m).

floor. This noise is caused by accumulation of the Brillouin signals from non-correlation (or non-sensing) sections along the FUT [34, 35]. As the nonlinear range of the BGS is mostly located on this noise floor, drastic improvement of the strain dynamic range cannot be expected by this method.

Here, we draw attention to the fact that the bell-shaped noise floor consists predominantly of the Brillouin signals from the non-sensing sections close to the sensing section (in other words, the closer the non-correlation sections are to the correlation peak, the greater their contributions to the noise floor become) [34, 35]. Therefore, if we intentionally lower the spatial resolution and include initially non-sensing sections into newly defined sensing section, the noise floor will be drastically diminished; as a result, the strain dynamic range will be greatly enhanced. Thus, SA-BOCDR has a trade-off relation between the strain dynamic range and the spatial resolution. We give experimental analysis on this nature in this paper.

### 3. Experimental setup

The experimental setup of SA-BOCDR is depicted in figure 1, which is essentially the same as that previously reported [26]. A continuous lightwave from a laser with a center wavelength

of  $1.55 \mu\text{m}$  was divided into two light beams: pump and reference. After amplified to  $\sim 26$  dBm using an erbium-doped fiber amplifier (EDFA), the pump light was injected into the FUT. The Brillouin-scattered Stokes light was then amplified to  $\sim 2$  dBm using another EDFA and coupled with the reference light for heterodyne detection. The reference light was amplified to  $\sim 1$  dBm after passing through a  $\sim 1$  km-long delay fiber. After converted into an electrical signal using a photodiode, the heterodyned signal was guided to an electrical spectrum analyzer (ESA; video bandwidth: 10 kHz, resolution bandwidth: 10 MHz). Using the narrowband-pass filtering function of the ESA, the change in the spectral power at 10.80 GHz was transmitted to an oscilloscope (OSC). The repetition rate was 100 Hz, and averaging was performed 512 times on the OSC to achieve a higher SNR.

As shown in figure 2, we used a 7.5 m-long silica single-mode fiber (SMF) with a BFS of 10.82 GHz at room temperature ( $20^\circ\text{C}$ ). A bending loss was applied near the open end to suppress the Fresnel reflection.

We performed two experiments: one was to measure the strain dynamic range of standard SA-BOCDR and to confirm the origin of its limitation, and the other was to investigate the trade-off relation between the strain dynamic range and the spatial resolution. In the first experiment, we set the

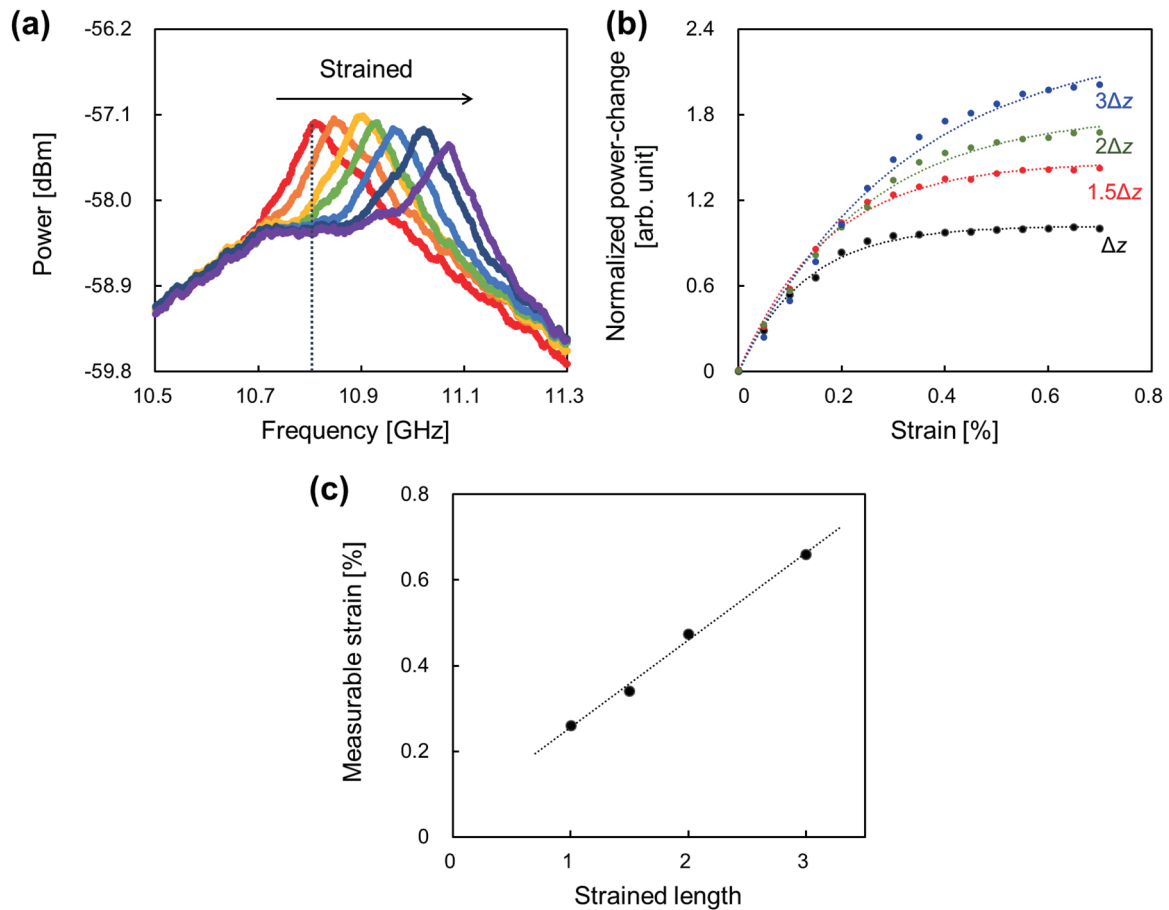


**Figure 4.** (a) BGSs measured at strains of 0–0.6% (step: 0.1%) when the strained length  $L_e$  was  $3\Delta z$ , where  $\Delta z$  is  $\sim 0.37$  m. (b) Normalized power changes plotted as functions of applied strain when the  $L_e$  values were  $\Delta z$ ,  $1.5\Delta z$ ,  $2\Delta z$ , and  $3\Delta z$ . The dotted curves are exponential fits. (c) Maximal measurable strain plotted as a function of  $L_e$ . The dotted line is a linear fit.

modulation frequency  $f_m$  and modulation amplitude  $\Delta f$  to 9.80–9.97 MHz and 0.27 GHz, respectively, which correspond to the measurement range  $d_m$  of  $\sim 10.3$  m and the theoretical spatial resolution  $\Delta z$  of  $\sim 0.37$  m according to equations (1) and (2). Distributed strain measurements were performed when strains of 0%–0.7% were applied to a  $\sim 0.37$  m-long section (same as  $\Delta z$ ). We simultaneously measured the BGSs in the strain range of 0%–0.3% when the correlation peak was located  $\sim 4.0$  m away from the end of the second-port SMF of an optical circulator (see figure 2;  $f_m$  was 9.89 MHz). In the second experiment, similar measurements of strain distributions and single-point BGSs were performed, but with elongated strained lengths  $L_e$  from  $\Delta z$  to  $3\Delta z$ , which can be regarded as intentionally lowered spatial resolutions.

#### 4. Experimental results

First, we present the results of SA-BOCDR-based distributed strain measurements when relatively large strains were applied. Figure 3(a) shows an example of the measured distribution of the spectral power change along the whole FUT when a 0.25% strain was applied to a  $\sim 0.37$  m-long section. The vertical axis was normalized so that the maximal power change became 1. The power change at the strained section was detected; a triangular shape (not rectangular)

indicates the correct operation of SA-BOCDR when the strained length equals the spatial resolution [28]. Similar measurements were performed at various strains in the range of 0%–0.7%. Figure 3(b) shows the measured dependence of the normalized power change (at the midpoint of the strained section) on applied strain. With increasing strain, the power change also increased, but the slope became gradually small (moderately fitted by an exponential curve). When strain was smaller than  $\sim 0.15\%$ , the dependence was almost linear, which agrees well with previous reports [26, 28]. However, in the strain range of approximately 0.15%–0.25%, the slope became smaller, which can still be used to measure strain because the power change and strain are in one-to-one correspondence. In contrast, once the strain exceeded  $\sim 0.25\%$ , the power change showed no significant growth and became almost constant. These results indicate that the use of the nonlinear range of the BGS slope is not an effective method for improving the strain dynamic range, which was slightly extended from 0.15% to 0.25% in this experiment. We also measured the BGSs while applying strains of 0%–0.3% to the  $\sim 0.37$  m-long section in the FUT. As shown in figure 3(c), with increasing strain, the spectral power at 10.80 GHz decreased when the applied strain was smaller than  $\sim 0.25\%$ , which corresponds to the trend in figure 3(b). However, it is clear that, when strain was larger, the spectral power stopped decreasing

because of the aforementioned bell-shaped background noise floor. This observation confirms that the strain dynamic range of SA-BOCDR is, even when the nonlinear range of the spectral slope is exploited, significantly restricted by this unique noise structure.

Subsequently, we show the results when the spatial resolution was lowered. Figure 4(a) shows the BGSs measured when the strains of 0–0.6% were applied to a 1.1 m-long section (corresponding to  $3\Delta z$ ) in the FUT. Unlike in the case where the strained length  $L_\varepsilon$  was  $\Delta z$ , the spectral power at 10.80 GHz decreased even when the applied strain was larger than 0.25%. This is because part of the noise floor shifted to higher frequency owing to the lowered resolution. This trend was basically the same when  $L_\varepsilon$  was  $1.5\Delta z$  and  $2\Delta z$ . Figure 4(b) shows the strain dependence of the normalized power change (at the midpoint of the strained section). Regardless of  $L_\varepsilon$ , the power change increased with increasing applied strain. The slope became gradually small, and the power change finally became almost constant, in the same manner as in figure 3(b). However, it is notable that, with increasing  $L_\varepsilon$ , the strain at which the power change became constant increased. In figure 4(c), as a function of  $L_\varepsilon$ , we finally plotted the maximal measurable strain, which we defined as the strain at which the power change reaches  $\sim 86.5\%$  of its saturated value. As  $L_\varepsilon$  increased, the maximal measurable strain increased almost linearly with a coefficient of  $\sim 0.2\%$  in this experiment. When the spatial resolution was three times lowered, the strain dynamic range was  $>0.6\%$ . Thus, we proved that the strain dynamic range can be improved at the cost of the spatial resolution in SA-BOCDR.

## 5. Conclusion

We clarified that SA-BOCDR has a trade-off relation between the strain dynamic range and the spatial resolution. To start with, we measured the BGSs when applied strains were larger than the previously reported upper limit ( $\sim 0.15\%$ ), and proved that the limited strain dynamic range is caused by the bell-shaped noise floor peculiar to the correlation-domain techniques. Then, by making use of the nature of this noise floor, we showed that the strain dynamic range can be improved at the cost of the spatial resolution. In the experiment, a strain dynamic range of  $>0.6\%$  was achieved with a spatial resolution lowered by three times. Considering that the spatial resolution of BOCDR is relatively high even in its standard configuration, such a lowered spatial resolution should still be useful in some applications. We have some other ideas to improve the strain dynamic range; for instance, by low-pass filtering the BGS, the dynamic range will be improved, but at the sacrifice of the measurement sensitivity. Using multiple spectral powers will be another approach, but the signal processing will be more complicated. Thus, we believe that our simple approach to widening the strain dynamic range of SA-BOCDR will be of significant use for practical applications in structural health monitoring in the future.

## Acknowledgments

This work was supported by JSPS KAKENHI Grant Numbers 17H04930 and 17J07226 and by a research grants from the Fujikura Foundation.

## ORCID iDs

Heeyoung Lee <https://orcid.org/0000-0003-3179-0386>  
 Kohei Noda <https://orcid.org/0000-0003-4976-9657>  
 Yosuke Mizuno <https://orcid.org/0000-0002-3362-4720>  
 Kentaro Nakamura <https://orcid.org/0000-0003-2899-4484>

## References

- [1] Agrawal G P 1995 *Nonlinear Fiber Optics* (Cambridge, MA: Academic)
- [2] Horiguchi T and Tateda M 1989 BOTDA-nondestructive measurement of single-mode optical fiber attenuation characteristics using Brillouin interaction: theory *J. Lightwave Technol.* **7** 1170
- [3] Kurashima T, Horiguchi T, Izumita H, Furukawa S and Koyamada Y 1993 Brillouin optical-fiber time domain reflectometry *IEICE Trans. Commun.* **E76-B** 382
- [4] Dong Y, Ba D, Jiang T, Zhou D, Zhang H, Zhu C, Lu Z, Li H, Chen L and Bao X 2013 High-spatial-resolution fast BOTDA for dynamic strain measurement based on differential double-pulse and second-order sideband of modulation *IEEE Photonics J.* **5** 2600407
- [5] Eloo D, Antman Y, Levanon N and Zadok A 2014 High-resolution long-reach distributed Brillouin sensing based on combined time-domain and correlation-domain analysis *Opt. Express* **22** 6453
- [6] Yang G, Fan X, Wang B and He Z 2018 Enhancing strain dynamic range of slope-assisted BOTDA by manipulating Brillouin gain spectrum shape *Opt. Express* **26** 32599
- [7] Dong Y, Wang B, Pang C, Zhou D, Ba D, Zhang H and Bao X 2018 150 km fast BOTDA based on the optical chirp chain probe wave and Brillouin loss scheme *Opt. Lett.* **43** 4679
- [8] Lalam N, Ng W P, Dai X, Wu Q and Fu Y Q 2018 Performance improvement of Brillouin ring laser based BOTDR system employing a wavelength diversity technique *J. Lightwave Technol.* **36** 1084
- [9] Mao Y, Guo N, Yu K L, Tam H Y and Lu C 2012 1-cm-spatial-resolution Brillouin optical time-domain analysis based on bright pulse Brillouin gain and complementary code *IEEE Photonics J.* **4** 2243
- [10] Garus D, Krebber K, Schliep F and Gogolla T 1996 Distributed sensing technique based on Brillouin optical-fiber frequency-domain analysis *Opt. Lett.* **21** 1402
- [11] Minardo A, Bernini R, Ruiz-Lombera R, Mirapeix J, Lopez-Higuera J M and Zeni L 2016 Proposal of Brillouin optical frequency-domain reflectometry (BOFDR) *Opt. Express* **24** 29994
- [12] Bernini R, Minardo A and Zeni L 2012 Distributed sensing at centimeter-scale spatial resolution by BOFDA: Measurements and signal processing *IEEE Photonics J.* **4** 48
- [13] Minardo A, Bernini R and Zeni L 2014 Distributed temperature sensing in polymer optical fiber by BOFDA *IEEE Photonics Technol. Lett.* **26** 387

- [14] Hotate K and Hasegawa T 2000 Measurement of Brillouin gain spectrum distribution along an optical fiber using a correlation-based technique -proposal, experiment and simulation *IEICE Trans. Electron.* **E83-C** 405
- [15] Mizuno Y, Zou W, He Z and Hotate K 2008 Proposal of Brillouin optical correlation-domain reflectometry (BOCDR) *Opt. Express* **16** 12148
- [16] Mizuno Y, He Z and Hotate K 2009 One-end-access high-speed distributed strain measurement with 13-mm spatial resolution based on Brillouin optical correlation-domain reflectometry *IEEE Photonics Technol. Lett.* **21** 474
- [17] Manotham S, Kishi M, He Z and Hotate K 2012 1-cm spatial resolution with large dynamic range in strain distributed sensing by Brillouin optical correlation domain reflectometry based on intensity modulation *Proc. SPIE* **8351** 835136
- [18] Mizuno Y, He Z and Hotate K 2009 Dependence of the Brillouin frequency shift on temperature in a tellurite glass fiber and a bismuth-oxide highly-nonlinear fiber *Appl. Phys. Express* **2** 112402
- [19] López-Gil A, Martín-Lopez S and Gonzalez-Herraez M 2017 Phase-measuring time-gated BOCDR *Opt. Lett.* **42** 3924
- [20] Song K Y and Choi J H 2018 Measurement error induced by the power-frequency delay of the light source in optical correlation-domain distributed Brillouin sensors *Opt. Lett.* **43** 5078
- [21] Mizuno Y, He Z and Hotate K 2009 Measurement range enlargement in Brillouin optical correlation-domain reflectometry based on temporal gating scheme *Opt. Express* **17** 9040
- [22] Mizuno Y, He Z and Hotate K 2010 Measurement range enlargement in Brillouin optical correlation-domain reflectometry based on double-modulation scheme *Opt. Express* **18** 5926
- [23] Jeong J H, Lee K, Song K Y, Jeong J and Lee S B 2012 Differential measurement scheme for Brillouin Optical Correlation Domain Analysis *Opt. Express* **20** 27094
- [24] Zhang C, Kishi M and Hotate K 2015 5,000 points/s high-speed random accessibility for dynamic strain measurement at arbitrary multiple points along a fiber by Brillouin optical correlation domain analysis *Appl. Phys. Express* **8** 042501
- [25] Mizuno Y, Hayashi N, Fukuda H, Song K Y and Nakamura K 2016 Ultrahigh-speed distributed Brillouin reflectometry *Light: Sci. Appl.* **5** e16184
- [26] Lee H, Hayashi N, Mizuno Y and Nakamura K 2016 Slope-assisted Brillouin optical correlation-domain reflectometry: Proof of concept *IEEE Photonics J.* **8** 6802807
- [27] Mizuno Y, Hayashi N, Fukuda H and Nakamura K 2017 Single-end-access distributed strain sensing with wide dynamic range using higher-speed Brillouin optical correlation-domain reflectometry *Japan. J. Appl. Phys.* **56** 072501
- [28] Lee H, Hayashi N, Mizuno Y and Nakamura K 2016 Operation of slope-assisted Brillouin optical correlation-domain reflectometry: comparison of system output with actual frequency shift distribution *Opt. Express* **24** 29190
- [29] Lee H, Mizuno Y and Nakamura K 2017 Measurement sensitivity dependencies on incident power and spatial resolution in slope-assisted Brillouin optical correlation-domain reflectometry *Sens. Actuators A* **268** 68
- [30] Lee H, Ochi Y, Matsui T, Matsumoto Y, Tanaka Y, Nakamura H, Mizuno Y and Nakamura K 2018 Distributed strain measurement and possible breakage detection of optical-fiber-embedded composite structure using slope-assisted Brillouin optical correlation-domain reflectometry *Appl. Phys. Express* **11** 072501
- [31] Zou L, Bao X, Ravet F and Chen L 2006 Distributed Brillouin fiber sensor for detecting pipeline buckling in an energy pipe under internal pressure *Appl. Opt.* **45** 3372
- [32] Villalba S and Casas J R 2013 Application of optical fiber distributed sensing to health monitoring of concrete structures *Mech. Syst. Signal Process.* **39** 441
- [33] Zhao X, Gong P, Qiao G, Lu J, Lv X and Qu J 2011 Brillouin corrosion expansion sensors for steel reinforced concrete structures using a fiber optic coil winding method *Sensors* **11** 10798
- [34] Song K Y, He Z and Hotate K 2006 Optimization of Brillouin optical correlation domain analysis system based on intensity modulation scheme *Opt. Express* **14** 4256
- [35] Song K Y, He Z and Hotate K 2007 Effects of intensity modulation of light source on Brillouin optical correlation domain analysis *J. Lightwave Technol.* **25** 1238
- [36] Mizuno Y, Zou W, He Z and Hotate K 2010 Operation of Brillouin optical correlation-domain reflectometry: Theoretical analysis and experimental validation *J. Lightwave Technol.* **28** 3300